water

MDPI

Article

Implications of a Large River Discharge on the Dynamics of a Tide-Dominated Amazonian Estuary

Ariane M. M. Silva [1], Hannah E. Glover [2], Mariah E. Josten [3], Vando J. C. Gomes [4], Andrea S. Ogston [3] and Nils E. Asp [5,*]

1 Graduate Program in Geology and Geochemistry, Federal University of Pará, Rua Augusto Corrêa, 01—UFPA-Guamá, Belém 66075-110, PA, Brazil
2 College of Engineering, Oregon State University (OSU), 101 Kearney Hall, Corvallis, OR 97331, USA
3 School of Oceanography, University of Washington (UW), Box 357940, Seattle, WA 98195-7940, USA
4 Coastal and Oceanic Engineering Faculty/Campus Salinópolis, Federal University of Pará (UFPA), Rua Raimundo Santana Cruz, s/n Bairro São Tomé, Salinópolis 68721-000, PA, Brazil
5 Institute for Coastal Studies, Federal University of Pará (UFPA), Alam. Leandro Ribeiro, s/n—Bairro Aldeia Campus UFPA, Bragança 68600-000, PA, Brazil
* Correspondence: nilsasp@ufpa.br

Abstract: Estuaries along the Amazonian coast are subjected to both a macrotidal regime and seasonally high fluvial discharge, both of which generate complex circulation. Furthermore, the Amazon River Plume (ARP) influences coastal circulation and suspended sediment concentrations (SSCs). The Gurupi estuary, located south of the mouth of the Amazon River, is relatively unstudied. This study evaluates how the Gurupi estuary dynamics respond to seasonal discharge and the varying influence of the ARP using cross-sectional and longitudinal surveys of morphology, hydrodynamics, and sediment transport. The Gurupi was classified as a tide-dominated estuary based on morphology and mean hydrodynamic conditions. However, the estuary was only partially mixed during both the wet and dry seasons. The tides propagated asymmetrically and hypersynchronously, with flood dominance during the dry season and ebb dominance during the rainy season. Seasonal variations of the ARP did not significantly affect the hydrodynamic structure of the lower Gurupi estuary. Estuarine turbidity maxima (ETM) were observed in both seasons, although the increase in fluvial discharge during the wet season attenuated and shifted the ETM seaward. Little sediment was delivered to the estuary by the river, and the SSCs were higher at the mouth in both seasons. Sediment was strongly imported during the dry season by tidal asymmetry. The morphology, hydrodynamics, and sediment dynamics all highlight the importance of considering both fluvial discharge and coastal influences on estuaries along the Amazon coast.

Keywords: Amazon coast; high fluvial discharge; suspended sediments; estuarine turbidity maxima; mangroves

Citation: Silva, A.M.M.; Glover, H.E.; Josten, M.E.; Gomes, V.J.C.; Ogston, A.S.; Asp, N.E. Implications of a Large River Discharge on the Dynamics of a Tide-Dominated Amazonian Estuary. *Water* **2023**, *15*, 849. https://doi.org/10.3390/w15050849

Academic Editor: Yiannis Savvidis

Received: 27 January 2023
Revised: 17 February 2023
Accepted: 20 February 2023
Published: 22 February 2023

1. Introduction

Rivers are the most important agents for transporting sediments to oceans [1,2]. The Amazon River is the largest sediment source to the ocean [3], carrying a load of about 1.2×10^9 t · yr^{-1} of sediments [4]. The Southeastern Amazon Coastal Zone (SACZ) is nearly 8000 km^2 and it stretches along approximately 480 km and covers the Brazilian states of Pará and Maranhão [5]. There are more than 20 tide-dominated estuaries in this region, where large amounts of mud were deposited during the Holocene [6–8]. However, these numerous, small Amazonian rivers do not contribute significantly to the sediment supply to the Atlantic Ocean because they carry a low SSC. These rivers are often called "blackwater rivers" because of the high levels of dissolved organic matter [9].

The transport and fate of sediment carried by these rivers is influenced by estuarine processes. The tidal range and fluvial discharge are fundamental controls on estuarine

processes, influencing the primary production, tidal wave propagation, estuarine turbidity maxima (ETM), salinity intrusion, and estuarine circulation [10–15]. The size of the drainage basin has a large impact on the timing and magnitude of fluvial discharge [6,16].

The Amazon River Plume (ARP) also influences the estuaries in the SACZ, especially by supplying fine sediments [6,17,18]. The surface area of the ARP reaches 1.5×10^6 km^2 and extends into the western tropical North Atlantic [19–21]. However, studies have shown that the ARP can also extend northwestward, penetrating approximately 100 km into the North Atlantic [17,19,22,23].

The Gurupi estuary is a large tide-dominated estuary in the eastern sector of the Amazon coast. This estuary provides an excellent opportunity to study the influence of river flow and the ARP on the hydrodynamics and morphodynamics of a macrotidal system. Recent research has been conducted on sediment dynamics and tidal propagation [6,18,24,25]. This study will evaluate how the large catchment area and high river discharge affect the hydrodynamics and morphology of the Gurupi River estuary. Additionally, we investigate the seasonally varying, fine-sediment contribution from the Amazon River Plume.

2. Study Area

The Gurupi estuary is a blackwater river [9] located between 1°3′50″ S and 1°51′50″ S and between 45°57′ W and 46°21′ W in the SACZ (Figure 1). The Gurupi estuary is characterized by widely developed mangrove forests [5], which cover an area of 1333.97 km^2. The main mangrove vegetation species are *Rhisophora mangle* (L.), *Avicennia germinans* (L.), and *Laguncularia racemosa* (L.) Gaertn. f. [5,25–27]. Additionally, in this sector, the coastal plateau can be found farther inland, including inactive bluffs, as the coastal plain prograde seaward during Late Holocene [5].

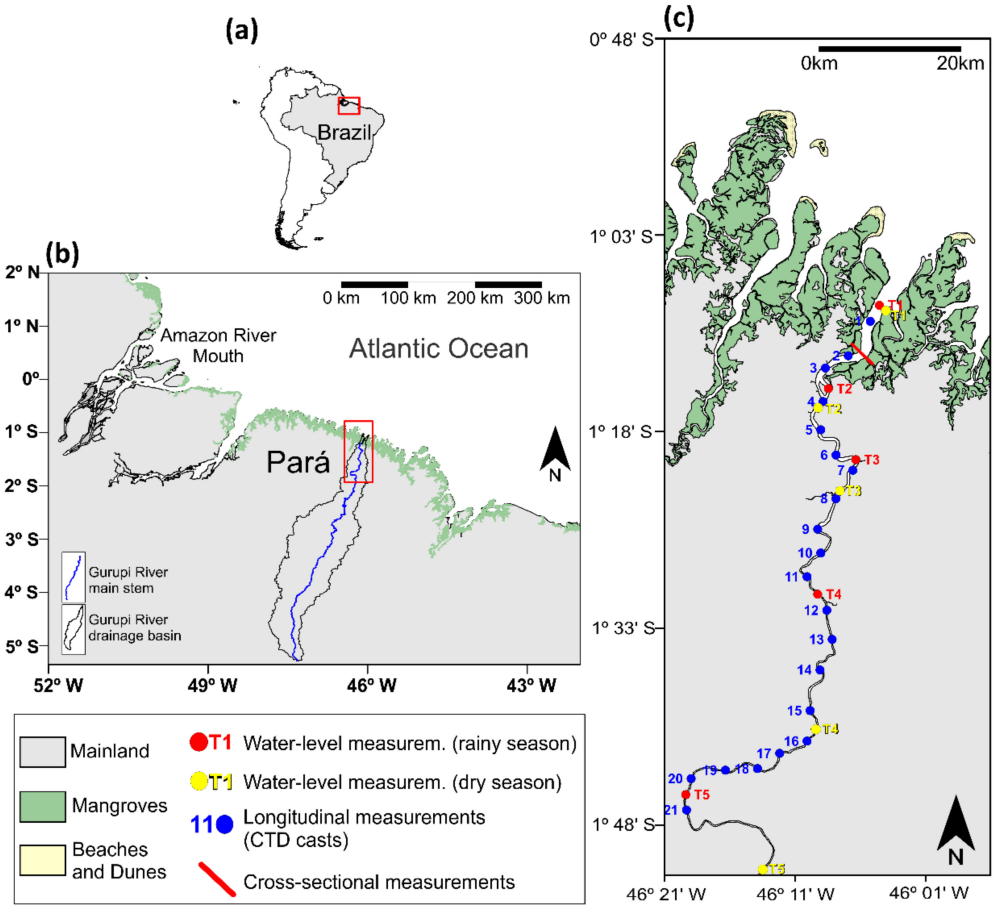

Figure 1. The location of (**a**) South America, (**b**) the Amazon Coastal Zone, and (**c**) the Gurupi River estuary, with sampling points.

The Gurupi River basin covers an area of 35,200 km^2 [7] and the river is approximately 700 km long [28]. The hydrographic basin area and the river profile have low relief, with elevations less than 100 m [29]. However, in the headland area, the elevation exceeds 450 m because of the Gurupi Mountain Range. The basin topography, geology, and hypsometry may contribute to the sediment production and erosion in the coastal zone. Though, the relatively minimal relief reduces the transport potential.

The region's climate is classified as hot and humid equatorial, with the rainy season from January to August, and the dry season from September to December. The climate is influenced by the variations in the position of the Intertropical Convergence Zone (ITCZ). The rainy season occurs when the ITCZ moves toward the coastal areas of the Maranhão, Pará, and Amapá states. In contrast, during the dry period, the ITCZ moves toward the Northern Hemisphere [7,30,31]. The average annual precipitation varies between 2.3 and 2.8 m [32]. The mean flow rate of the Gurupi River is 472 $m^3 \cdot s^{-1}$, and the flow rate is estimated to be approximately seven times greater in the rainy season than in the dry season [18,33]. The mean discharge over a 10-year period (2005–2014) was 161 $m^3 \cdot s^{-1}$ in November, and 1137 $m^3 \cdot s^{-1}$ in April [34]. The maximum tidal range is 5.6 m (in this study).

3. Materials and Methods

3.1. Fixed Instruments

The water levels were obtained using tidal gauges of the Onset/HOBO® (Bourne/MA—USA) U20-002-Ti model pressure sensors sampling at 1 Hz. These tidal gauges were installed at five points along the estuary, with approximately 20 km of spacing between locations (Figure 1c). The instruments were deployed in both the dry and rainy seasons to identify the propagation and deformation of the tide during low and high fluvial discharge. The location of the tidal gauges differs within the seasons, as tides propagate farther during the dry season. The tidal gauges were installed during the first day of the campaign and removed on the last day to ensure complete tidal cycle records.

3.2. Boat-Based Longitudinal Surveys

Bathymetric data were collected along the estuary during the rainy (i.e., May 2012) and dry (i.e., November 2012) seasons, to examine the bottom morphology and calculate the cross-sectional areas. Data were collected from a small boat, using a Furuno® 4100 echo sounder, a Global Positioning System (GPS) device, GPSmap 60CSx model from Garmin®, and a notebook.

Longitudinal surveys of hydrodynamic and sedimentology aspects along the Gurupi estuary were conducted during the rainy (April) and dry (November) seasons to capture seasonal variability. Vertical profiles in the water column were collected using a Sea and Sun model 90M CTD probe (conductivity, temperature, and depth), which was additionally equipped with a Seapoint® bulkhead turbidity sensor. The water column profiles were approximately 5 km apart, totaling 21 measurement locations (Figure 1c).

The suspended sediment concentration (SSC) was estimated by collecting water samples using a Niskin sampler at ~30 cm below the surface. Sampling was performed simultaneously with CTD casts. The water samples were stored in plastic bottles, and the SSC was determined through filtration, using a vacuum pump and glass fiber filters with 44 mm in diameter with 0.6 µm porosity [35]. The turbidity values were related to the SSC using a large dataset of samples (~180 casts/samples), including other neighboring estuaries according to [15]. This resulted in a quadratic polynomial correlation between calculated SSC from physical samples and measured FTU from the CTD casts (SSC ($g \cdot L^{-1}$) = 0.0000008 $(OBS)^2$ + 0.0006 (OBS) + 0.0221), R^2 = 0.805). This equation was used to convert turbidity into SSC [18].

3.3. Boat-Based Transversal Surveys

Flow and current velocity data were measured using an Acoustic Doppler Current Profiler (ADCP) model workhorse monitor (1200 kHz) Teledyne®. A single transect was occupied ~20 km from the coastal line during the rainy and dry seasons (Figure 1c). The vessel traversed the transect every 30 min for a 13-hour period to capture the tidal cycle.

3.4. Data Processing

The morphology was analyzed using bathymetric data, Landsat 5 TM satellite imagery, and SRTM (Shuttle Radar Topography Mission) data to establish the watershed boundaries and water pathways. These datasets were integrated using Surfer 13 (Golden Software, Golden/CO—USA) to construct a digital elevation model (DEM). Subsequently, bathymetric and topographic profiles were extracted, and the area and volume were calculated. Longitudinal survey data were analyzed using SDA Sea & Sun Technology GmbH (Trappenkamp, Germany), Microsoft Excel, Grapher 12, and Surfer 13 software. Transverse survey data were processed using the WinRiver II softwares.

The residual fluxes of sediment and water were estimated following [2,36]. Since the cross-sectional area varies with the tide, a sigma coordinate was used to replace the depth with values between 0 at the surface and 1 at the bed (σ = z/h) [2,36,37]. The SSC transects were linearly interpolated using the CTD profiles. The residual flux was calculated by assuming the following:

$$F = \left\langle \int ucdA \right\rangle, \tag{1}$$

where u is the velocity, c is the concentration (suspended sediment or salt), dA is the cross-sectional area (divided into 18 grid cells), and $\langle\ \rangle$ represents the tidal averaging. The velocity and concentration vary across-channel (y), vertically (σ), and temporally (t). The transect-wide fluxes were calculated from the salinity and turbidity values, measured by the CTD, and assigned to ADCP ensembles according to [36,38]. Temporal and spatial data gaps were filled using linear interpolation.

For the residual flux of sediment, missing values were estimated by cubic interpolation of SSC. The residual flux was decomposed following [2,36,39], by assuming the following:

$$F = u_0 c_0 A_0 + \int u_1 c_1 dA_0 + \left\langle \int u_2 c_2 dA \right\rangle = F_R + F_E + F_T, \tag{2}$$

$$u_0 = \frac{\left\langle \int udA \right\rangle}{A_0}, c_0 = \frac{\left\langle \int cdA \right\rangle}{A_0}, u_1 = \frac{\langle udA \rangle}{dA_0} - u_0, c_1 = \frac{\langle cdA \rangle}{dA_0} - c_0, \tag{3}$$

$$u_2 = u - u_0 - u_1, c_2 = c - c_0 - c_1, \tag{4}$$

where F_R is generally interpreted as river advection, F_E is generally interpreted as estuarine exchange flux, and F_T is the residual term containing other processes such as tidal pumping, local erosion, and deposition.

The estuarine circulation and salinity structures were classified using the parameterization proposed by [15], also applied in [36,38]. According to [15], this parameterization allows the classification of estuaries using the principal forcing variables, the tidal velocity, and the freshwater flow. This classification relies on the freshwater Froude number and the Mixing number. The freshwater Froude number represents the fluvial forcing (freshwater input) and is calculated as follows:

$$F_{Rf} = \frac{U_R}{\sqrt{\beta g S H}}, \tag{5}$$

where U_R is the river velocity, β is 7.7×10^{-4} (β = coefficient of salinity), g is the gravitational acceleration, S is the oceanic salinity, and H is the water depth. The Mixing number (M) describes the tidal forcing (vertical tidal mixing) and is calculated as follows:

$$M^2 = \frac{C_D U_T^2}{\omega N_0 H^2}, \quad (6)$$

where C_D is the drag coefficient, U_T is the tidal velocity, ω is the tidal frequency, and N_0 is the buoyancy frequency from the maximum top-to-bottom salinity variation [15,36,38]. The drag coefficient was calculated according to [40].

3.5. Statistics Analyses

Additional statistical analyses were used to determine whether there were significant differences between the seasonal data of salinity and SSC from the two sample groups (April and November). The analyses were performed in the R software by applying the Vegan and ggplot2 packages [41–43]. The normality of all data were checked using the Shapiro–Wilk test. As the data were non-parametric and unpaired, the Mann–Whitney U test was used [44–46]. For both tests, the Shapiro–Wilk test and the Mann–Whitney U test, a significance level of 95% (p-value = 0.05) was adopted for the analysis.

4. Results

4.1. Estuarine Morphology

The Gurupi is a typical coastal plain estuary, presenting a funnel-like lower estuary, with tidal meanders along the middle sector and progressively narrowing upstream. Mangroves border the estuary longitudinally from the middle sector to the lower sector. The Gurupi is relatively shallow, with an average depth of ~6 m (Figure 2), reaching 13 m near the mouth (see profile 1 in Figure 2).

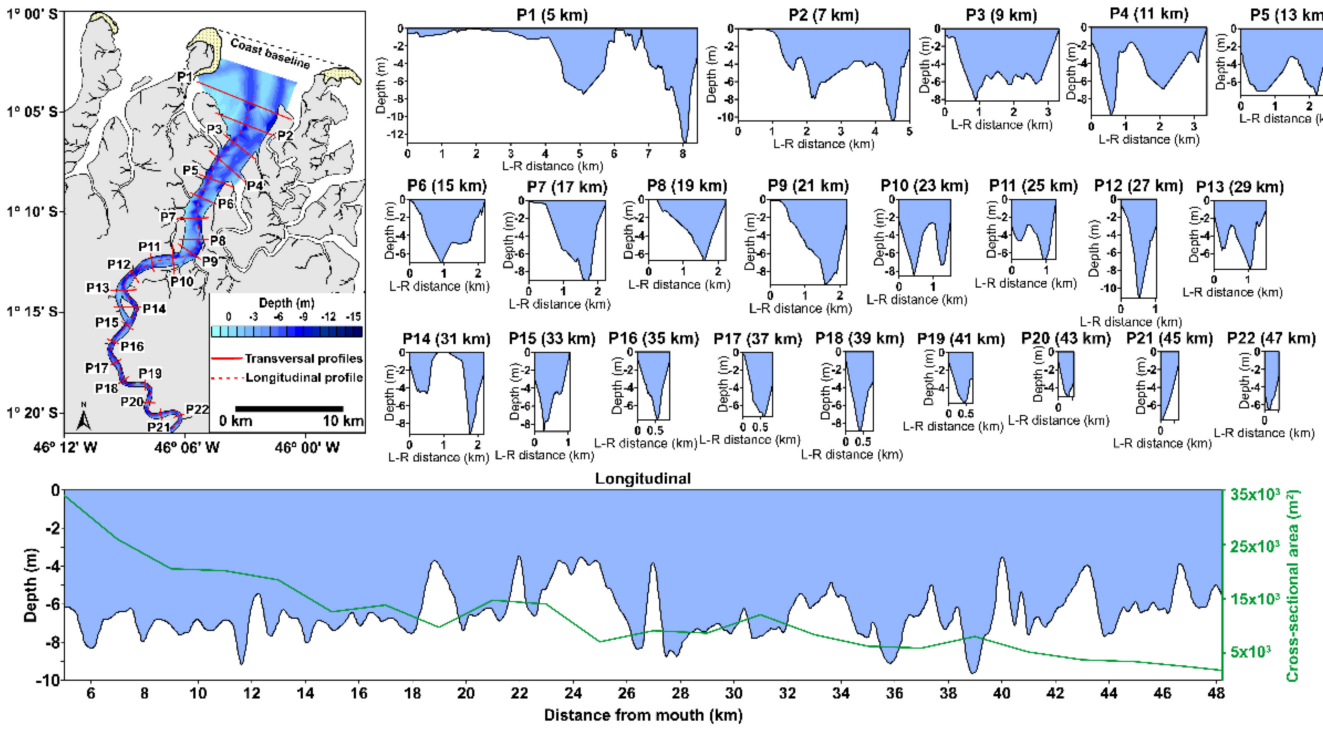

Figure 2. Bathymetric profiles showing the morphology of the Gurupi estuary. The red lines show the location of the transect. The green line shows the variation of the cross-sectional area along the estuary. Seasonal bottom morphology changes are not considered.

The bottom morphology and depths vary along the estuary with the formation of W-shaped channels in areas such as profiles P1 to P6, P10, and P11 (Figure 2). Additionally, a V-shape cross-section is observed on the upper estuary (P15–P22). No substantial seasonal morphological changes were observed. However, the seasonal river flood results in deeper waters in the upper estuary, whereas the water level might increase by ~3 m during the rainy season. This resulted in an apparent morphological difference (comparison of Figure 3a,b with Figure 3d,e). Additionally, these profiles may not follow the precise thalweg, resulting in apparently different profiles for each season.

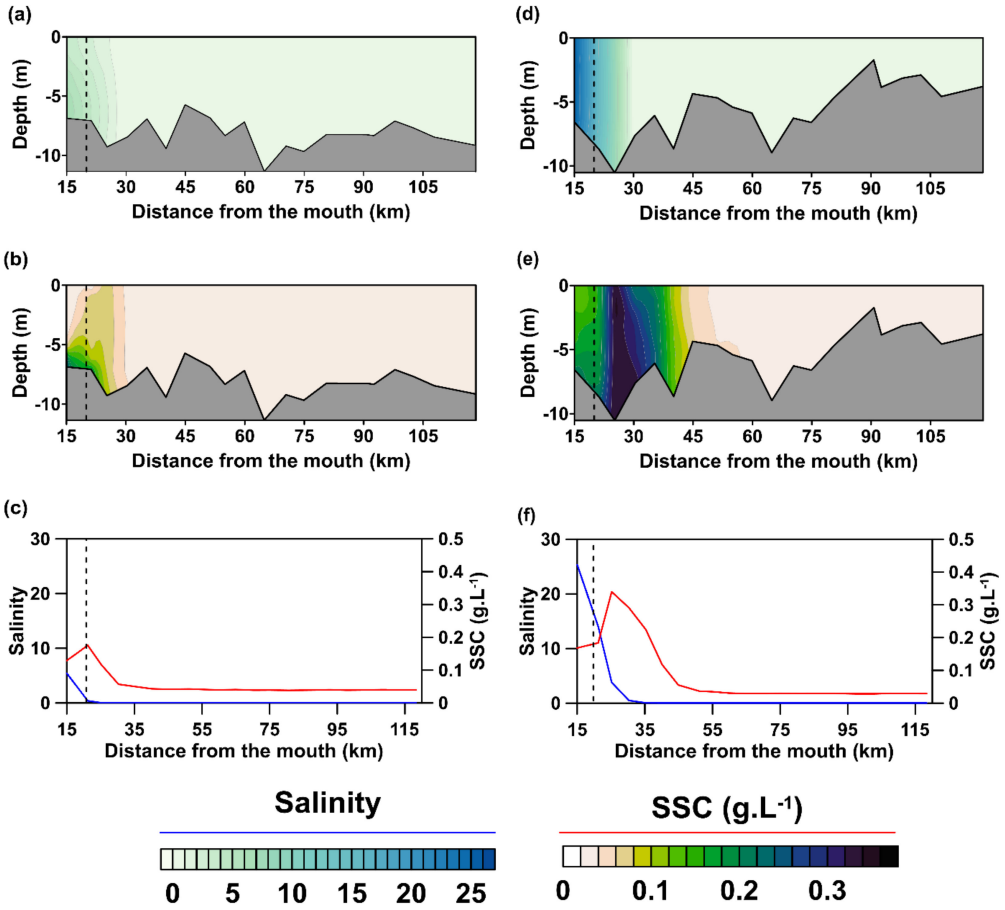

Figure 3. Longitudinal variation of salinity and SSC during the rainy (**a**–**c**) and dry (**d**–**f**) seasons (modified from [18]). The dashed line represents the location of the cross-sectional profile with ADCP. Notice that the location of the cross-section profile is the same for both seasons.

4.2. Suspended Sediment Concentration and Salinity

Suspended sediment concentration (SSC) and salinity were higher near the mouth. However, values were seasonally different. During the rainy season, SSC values ranged from 0.17 g · L^{-1} to 0.03 g · L^{-1}, from the mouth to the head of the estuary. Furthermore, the greater SSC values were recorded near the mouth and a concentration of 0.04 g · L^{-1} was consistently recorded along the middle and upper estuary. The observed salinity varied between 5.4 in the lower estuary to ~0 at ~30 km (Figure 3a–c).

During the dry season, the SSC values were substantially higher than in the rainy season, ranging from 0.34 g · L^{-1} to 0.28 g · L^{-1}. During the dry season, increased SSC was observed along most of the estuary, and a lesser SSC was only observed at ~51 km from the mouth. As expected, the salinity levels were higher during the dry season than in the rainy season. The maximum salinity was 25 and reached ~0 at 40 km from the mouth (Figure 3d–f). Variations of salinity and SSCs were greater in the lower sector of the Gurupi estuary (until ~30 km from the mouth).

The Mann–Whitney U test was used to check if these seasonal variations were significant. Regarding salinity, the Mann–Whitney U test showed a significant seasonal difference (W = 9.5; *p*-value = 0.02978). These variations were expected due to the reduction in rainfall and river flow during the dry season, which directly impacts the salinity. The SSC also differed between the dry and rainy seasons (W = 3; *p*-value = 0.01515). Local fluvial waters have a low SSC, and increased fluvial discharges result in SSC dilution.

4.3. Tidal Patterns in Estuary Fluxes

The instantaneous fluvial discharge was also compared to the current velocities and net residual discharge. During the rainy season, the maximum values of total discharge during the flood and ebb phases were 6863 $m^3 \cdot s^{-1}$ and 4435 $m^3 \cdot s^{-1}$, respectively. The maximum values of current velocity during the flood and ebb phases were 0.95 $m \cdot s^{-1}$ and 0.76 $m \cdot s^{-1}$, respectively (Figure 4a).

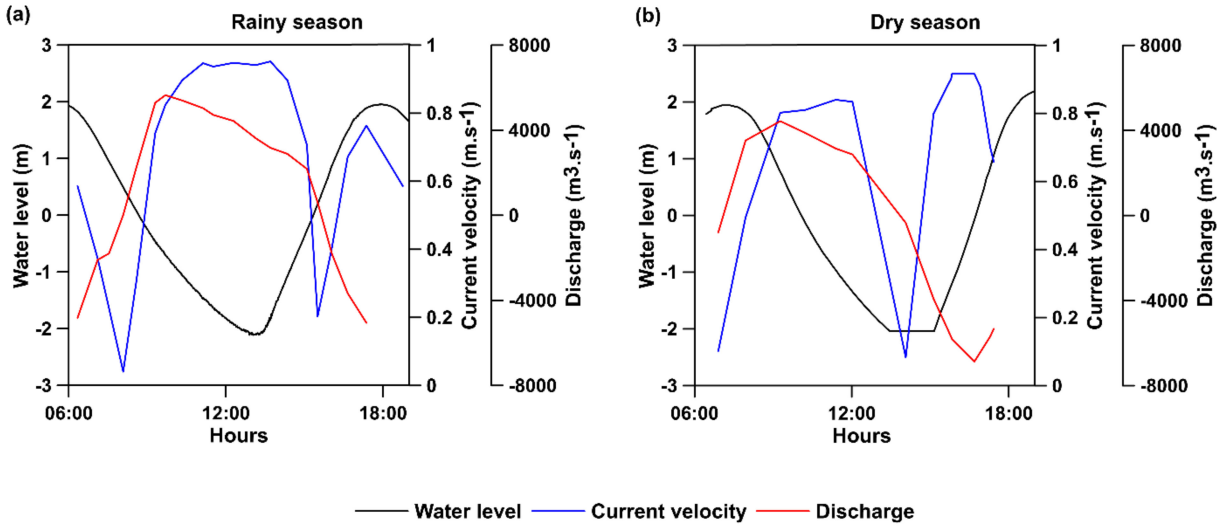

Figure 4. Hydrodynamics in the cross-sectional area comparing the discharge (red line) and the current velocity (blue line), during the rainy (**a**) and dry (**b**) seasons. The black line shows the water level variation.

During the dry season, the maximum total discharge was greater during the ebb (5647 $m^3 \cdot s^{-1}$) than during the flood phase (5505 $m^3 \cdot s^{-1}$). The maximum current velocity was 0.84 $m \cdot s^{-1}$ and 0.93 $m \cdot s^{-1}$ during the ebb and flood phases, respectively (Figure 4b).

Vertical (surface–bottom) variations of salinity and SSC were observed in both seasons with greater values near the bottom for both variables. As expected, the salinity level was consistently greater during the dry season. At the transect locations, thew salinity values were close to zero during the rainy season and reached 14.5 during the dry season. For the dry season, variations along the tidal cycle follow the expected pattern of higher values during the flood, in comparison with the ebb phase (Figure 5b). For the rainy season, there was a small peak of salinity (i.e., 1.09) during the beginning of the ebb, which is associated with the flushing of large mangrove areas with salt-rich sediments (Figure 5a). Further, surface–bottom variations were noticeable, especially during the dry season, when differences reach up to five between the saltier bottom waters and the surface, during the onset of the ebb phase.

In contrast, the SSC was substantially greater during the dry season in comparison with the rainy season, considering both cross-sectional and longitudinal measurements. The SSC values were about 0.11 $g \cdot L^{-1}$ at the surface and 0.24 $g \cdot L^{-1}$ at the bottom during the rainy season. During the dry season, the SSC values were 0.20 $g \cdot L^{-1}$ and 0.24 $g \cdot L^{-1}$ at the surface and bottom, respectively (Figure 5).

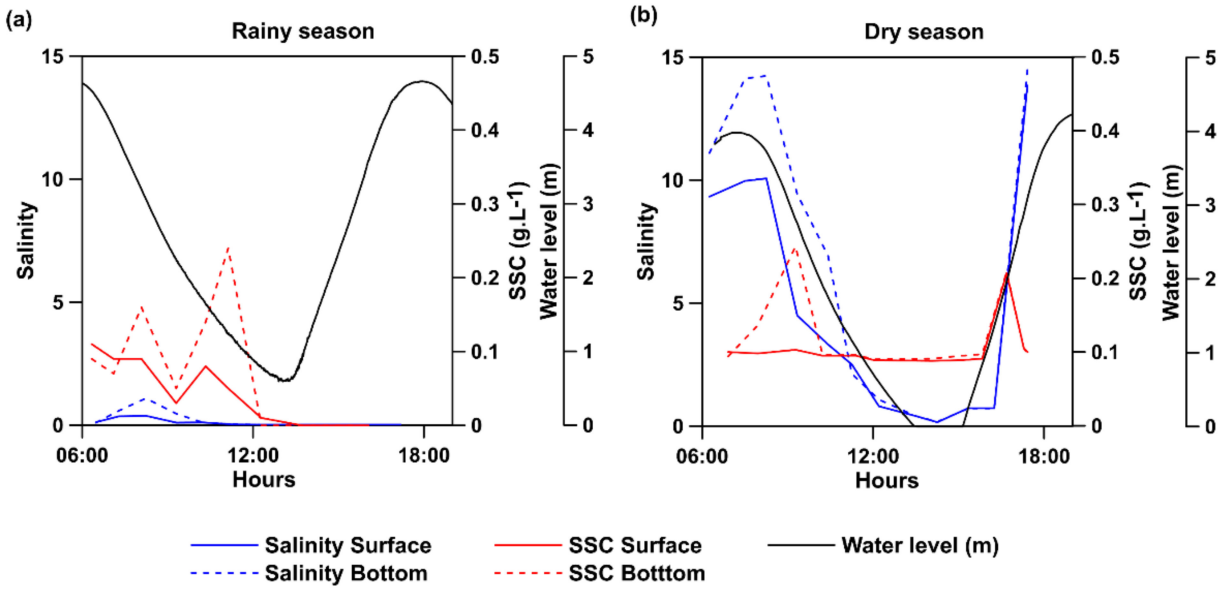

Figure 5. Hydrodynamics in the cross-sectional area comparing the salinity and SSC data during the rainy (**a**) and dry (**b**) seasons. The blue line shows the salinity level at the water surface (solid line) and bottom (dashed line). The red line shows the SSC data at the water surface (solid line) and at the bottom (dashed line).

4.4. Estuary Fluxes

4.4.1. Net Water and Sediment Fluxes

The net residual water and sediment discharges differed significantly between the seasons. The ratio of river discharge (Q) (m^3)/tidal cycle was 0.007 $m^3 \cdot s^{-1}$ (seaward) and -0.027 $m^3 \cdot s^{-1}$ (landward) during the rainy and dry seasons, respectively. The mean water flux led to a positive flux gradient during the rainy season. However, during the dry season, the Gurupi estuary showed a higher flux peak during the flood phase with a net landward flux (Figure 6).

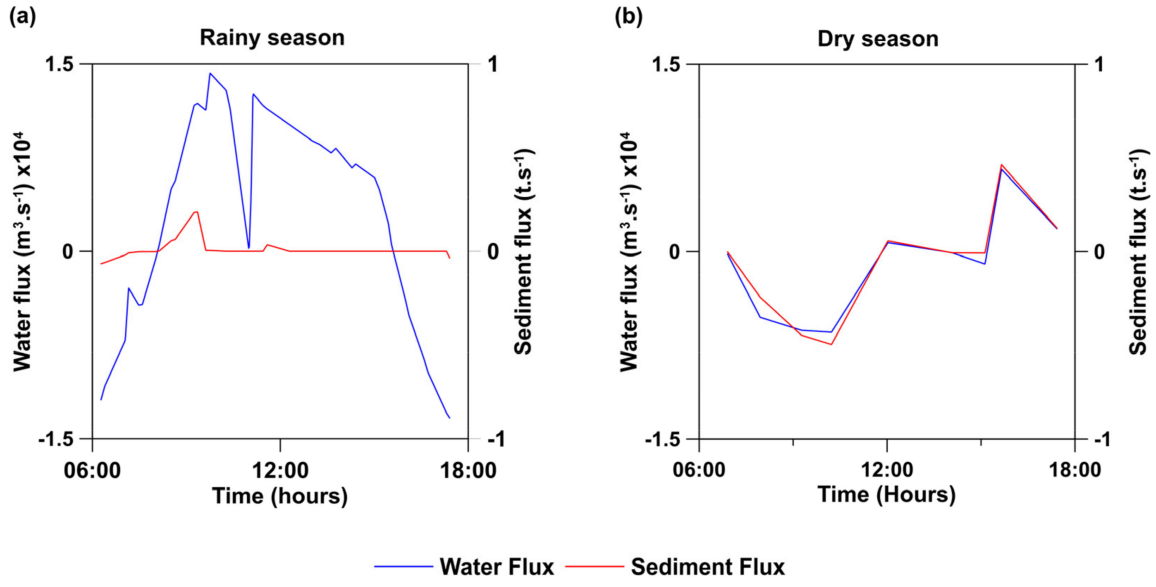

Figure 6. Water (blue line) and sediment (red line) fluxes for the Gurupi estuary during the rainy season (**a**) and dry season (**b**).

The sediment flux for the rainy season ranged from -0.06 t $\cdot$ s^{-1} to 0.21 t $\cdot$ s^{-1}, indicating processes of importation and exportation, respectively. The mean sediment flux was 0.07 t $\cdot$ s^{-1}, indicating net sediment export to the estuary. The sediment flux during the dry season ranged from -0.49 t $\cdot$ s^{-1} (import) to 0.46 t $\cdot$ s^{-1} (export). The mean sediment flux was -0.07 t $\cdot$ s^{-1}, indicating net sediment import to the estuary.

4.4.2. Sediment Flux Decomposition

The sediment flux decomposition shifted seasonally by one order of magnitude. During the rainy season, the river advection (F_R), estuarine exchange (F_E), and residual tidal (F_T) processes all led to an export of sediment. In contrast, during the dry season, the fluvial and tidal processes drove the importation of sediments (Figure 7). The flux decomposition showed that the estuarine exchange was the primary mechanism of transport for both seasons.

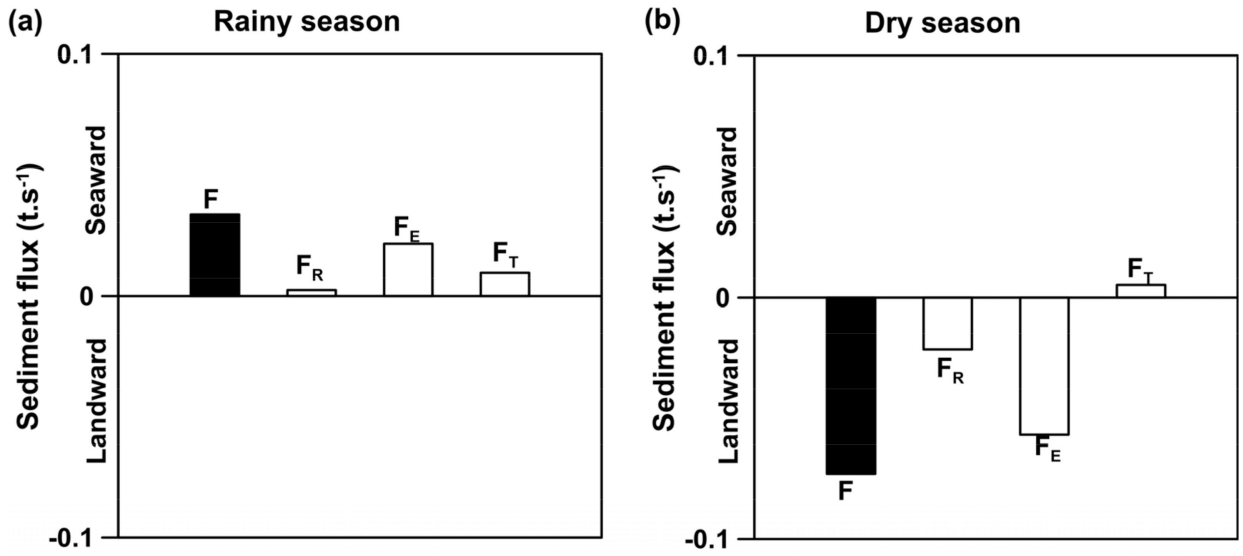

Figure 7. Sediment flux decomposition for Gurupi estuary during the rainy (**a**) and dry (**b**) seasons. The first column (black) represents the total sediment flux (F). F_R, F_E, and F_T represent river flux, estuarine exchange, and tidal residual flux, respectively.

4.5. Tidal Propagation

In the lower area of the Gurupi estuary, the tidal range increased as the estuary became narrower toward its head. At the mouth, the maximum measured tidal range was 5.6 m and 5.1 m, during the rainy and dry seasons, respectively (Figure 8a,b). In the lowermost section of the estuary, the water level and current velocities were relatively synchronous. With the tidal propagation at the estuarine funnel, some amplification was observed during the dry season (Figure 8b). Upstream of the Gurupi estuary, the river discharge becomes dominant, and the tidal range was damped (Figure 8a,b), mainly due to frictional effects from the narrowing cross-section (see tidal gauge T5—Figure 1). However, the river discharge is an important frictional factor in the tidal propagation upstream, especially during the rainy season, resulting in a stronger tidal attenuation (Figure 8a), in comparison to the dry season (Figure 8b).

The Gurupi estuary also presents an asymmetric pattern regarding the tidal phase duration, with the ebb longer than the flood phase during both seasons (Figure 8c,d). However, during the rainy season, the phase asymmetry is increased, due to the increased fluvial discharge.

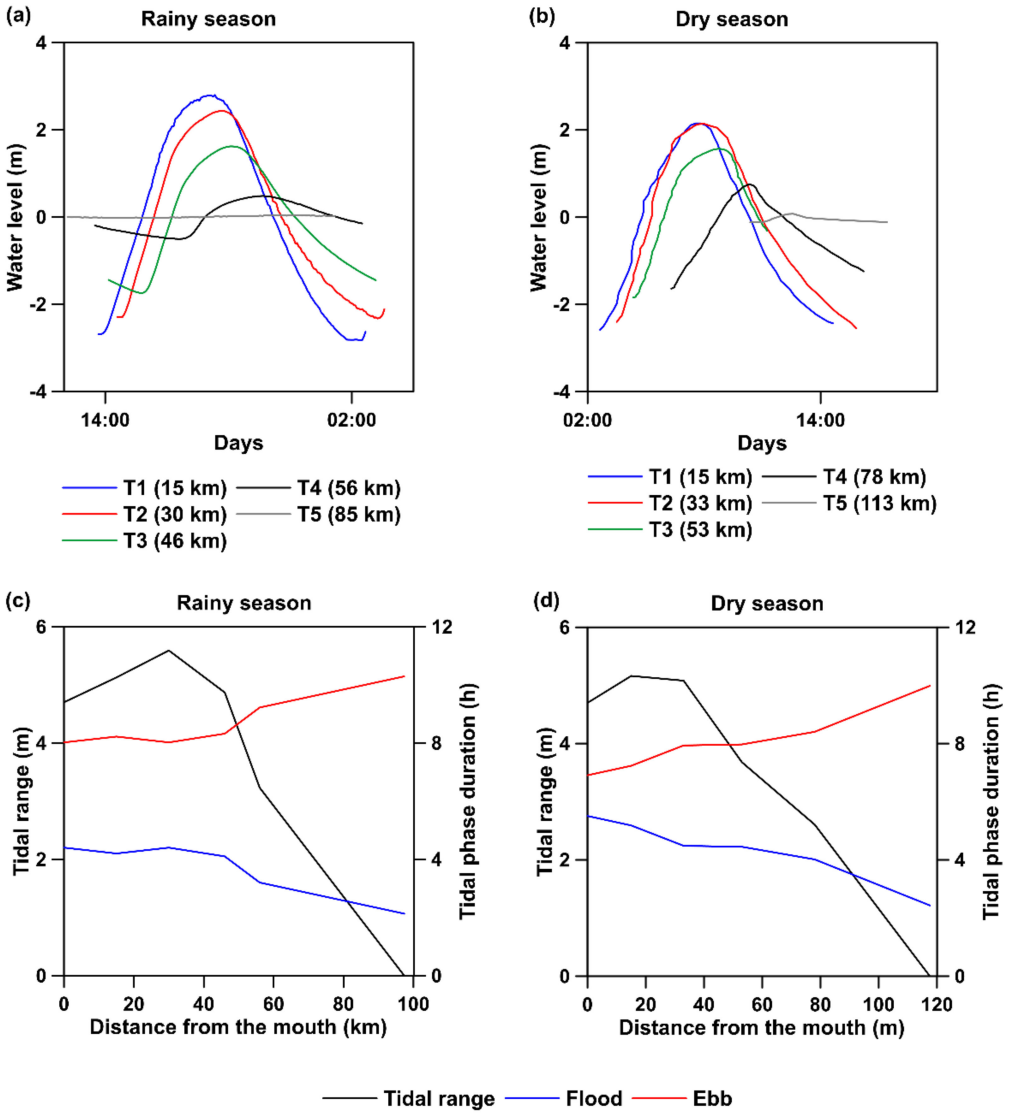

Figure 8. Water level oscillation along the Gurupi estuary. Panels (**a**,**b**) show the oscillation during rainy and dry seasons, respectively. Panels (**c**,**d**) show the longitudinal variation of tidal range and tidal phase duration during rainy and dry seasons.

5. Discussion

Overall, the results place the Gurupi as a tidal-dominated estuary, where estuarine exchange dominates sediment transport processes. The local fluvial discharge and ARP impact the seasonal variations of flow and stratification, which control sediment import and export. These competing tidal and fluvial processes are especially apparent during the rainy season.

5.1. ETM Formation and Implications for Sediment Dynamics

In tidal-dominated estuaries, fluvial suspended sediment transport and tidal processes tend to form a zone referred to as Estuarine Turbidity Maximum (ETM), where the SSC is greater [47,48]. The location, concentration, and size of the ETM will vary with the estuarine conditions. In the Gurupi, an ETM zone was observed in both seasons. During the dry season, the ETM zone was located between 20–35 km from the mouth and the SSC was significantly elevated, reaching up to 0.335 g $\cdot$ L^{-1} at the surface. However, during the rainy season, the ETM zone shifted to 15–25 km from the mouth and the maximum SSC only reached 0.101 g $\cdot$ L^{-1} at the surface. This compression of the ETM can be explained by the increase in river discharge during the rainy season. The interaction between the

tidal wave and the strong river discharge compressed the ETM into the estuary. Similar behavior was observed in the Gironde estuary [11,49], Colombia river estuary [11,50], Humber estuary [51], and Caeté estuary [6].

During this rainy season, low amounts of suspended sediment were being transported by the Gurupi River, despite the large river discharge. In addition, the increased river flow and the ebb-phase dominance inhibited the entry of sediments from offshore sources, especially the ARP. Consequently, the SSC was generally lesser throughout the estuary during the rainy season. The net transport of sediment through the Gurupi estuary remains unclear. The data indicate that the Gurupi estuary could be importing suspended sediments during this period; however, the concentrations and magnitude of the values observed were very low and are therefore, within the margin of error.

Estuarine conditions were significantly different during the dry season, when the river flow is ~7 times lower than during the rainy season. There was a greater contribution of freshwater and sediment from offshore sources. Consequently, higher values of SSCs and an expansion of about ~5 km of the ETM zone were observed, with a shift landward. We note that in this period, the SSC peak of the ETM zone was landward of the point where the cross-sectional profile was performed. There was a strong, net import of sediment, including a tidally invariant landward flux (Fr in Figure 7b). Generally, this Fr term is associated with the net, near-surface fluvial discharge [2,36]. However, in the Gurupi, this term demonstrates the importance of the persistent supply of sediment from the ARP.

Overall, the seasonal patterns of SSCs were consistent with the ARP role in the SSC dynamics and ETM formation. The ARP expands to the southeast shelf due to the prevailing winds and the ITCZ seasonal migration [52]. Consequently, the SSC from the Amazon River is carried into estuaries along the southeastern Amazon coast [6,18]. The data presented here demonstrate that the ARP is also important for the Gurupi estuary. However, since the Gurupi estuary is more than 400 km away from the Amazon River mouth, the seasonal ARP fluctuations are less dramatic than those observed in estuaries nearer the Amazon River mouth, such as the Mocajuba and even the Caeté [6,18,53].

5.2. Estuarine Circulation

Estuaries can be classified based on the geomorphological aspects as fjords (deep estuaries), drowned river valleys, bar-built estuaries, and rias, among others. However, the shape of the along-estuary salinity gradient is an important driver of estuarine processes, and this structure can also be used to classify estuaries [54]. The salinity and vertical stratification are determined by the geomorphology, freshwater flow, and tides [55]. In this context, estuaries can be classified as a salt wedge, weakly stratified or partially mixed, heavily stratified, and well-mixed, based on the relative strength of tidal mixing versus freshwater discharge [56].

The Gurupi estuary is classified as partially mixed (Figure 9), which is consistent with the observed structures. During the rainy season, the Mixing number (M) was 0.84 and the freshwater Froude number (F_{rf}) was 0.01. During the dry season, the values were 0.91 and 0.02 for the Mixing number (M) and freshwater Froude number (F_{rf}), respectively. However, a well-mixed classification would be expected for tide-dominated estuaries. In partially mixed estuaries, the salinity is higher at the mouth and decreases upstream. Additionally, the vertical layers of water mix at all depths, although the bottom layer is saltier than the top [57], as observed in the Gurupi estuary (Figures 3 and 5). Although the estuarine circulation is partially mixed based on the cross-sectional measurements (Figure 5), the salinity difference between the bottom and surface is only apparent during the ebb. During the flood tide, the estuary is rather well-mixed (Figure 3).

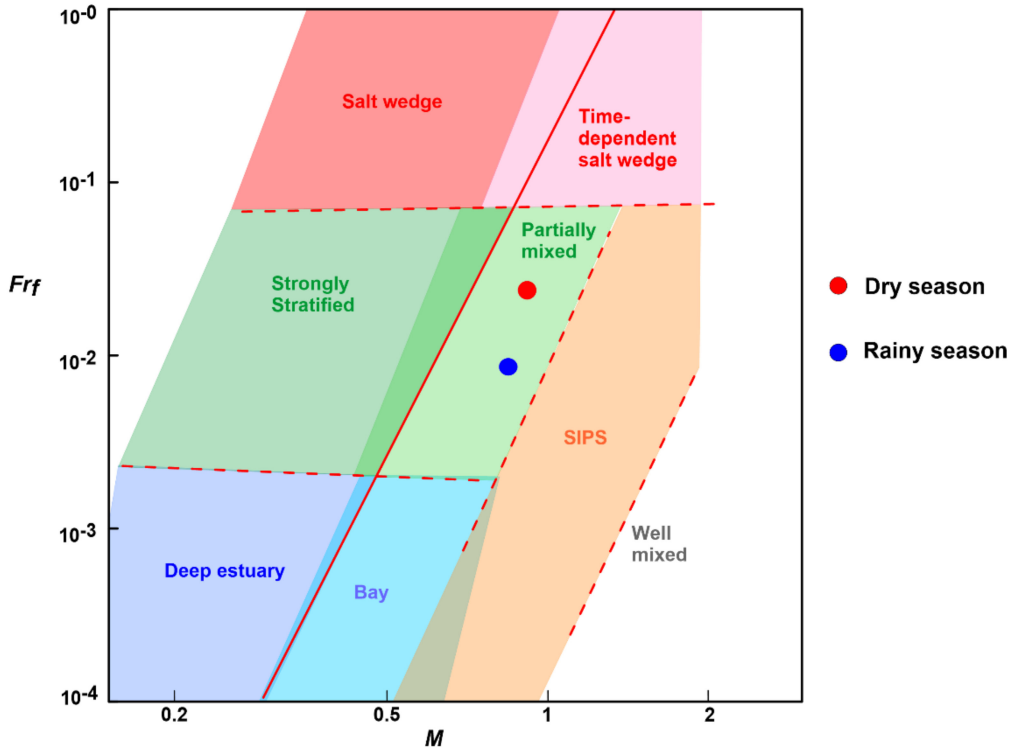

Figure 9. The Gurupi estuary in estuarine parameter space (diagram following the classification of [15]). The blue point represents the rainy season and the red point represents the dry season.

5.3. Comparison to Other Amazonian Estuaries

This investigation of the Gurupi estuary emphasizes the variability in estuaries within the SACZ. The Gurupi estuary is one of the largest Amazon estuaries [58], and because of its funnel-shape morphology, the presence of a W-shaped channel, and a rather wide and shallow basin, the Gurupi estuary is comparable with the Caeté and Urumajó estuaries [6,18,25]. From a morphologic perspective, the Gurupi is a typical tide-dominated estuary. However, the hydrodynamics do not uniformly match those in other tide-dominated estuaries.

A comparison with other typical tide-dominated estuaries (equilibrium estuaries) along the eastern sector of the Amazon coast was used to try to categorize estuaries along the Amazon coast based on the relative tidal prism (tidal prism/total estuarine volume) versus the fluvial discharge into the system (Figure 10). Based on recent investigations [6,18,24], it is considered that typical tide-dominated estuaries (equilibrium estuaries) along the eastern sector of the Amazon coast have tidal prisms between half and two-thirds of the total estuarine water volume. For the SACZ, three estuaries have been considered as representative of equilibrium estuaries, which include the Gurupi, Urumajó, and Caeté estuaries [18]. Using a linear relationship to fit the data of river discharge and relative tidal prism ($y = -0.0002x + 0.6738$), an R-squared value of 0.98 was obtained. It shows that during the rainy season, the channel (residual) estuarine volume of the Gurupi estuary overcomes the tidal prism, and during that period, the Gurupi estuary is not a typical tide-dominated estuary. Globally, these findings show that large river estuaries are subject to a critical balance between tidal prism and fluvial discharge, which determine if the estuary is either importing or exporting sediments, whereas slight changes in fluvial discharge, due to, for instance, climate changes or water uses, might change the balance substantially.

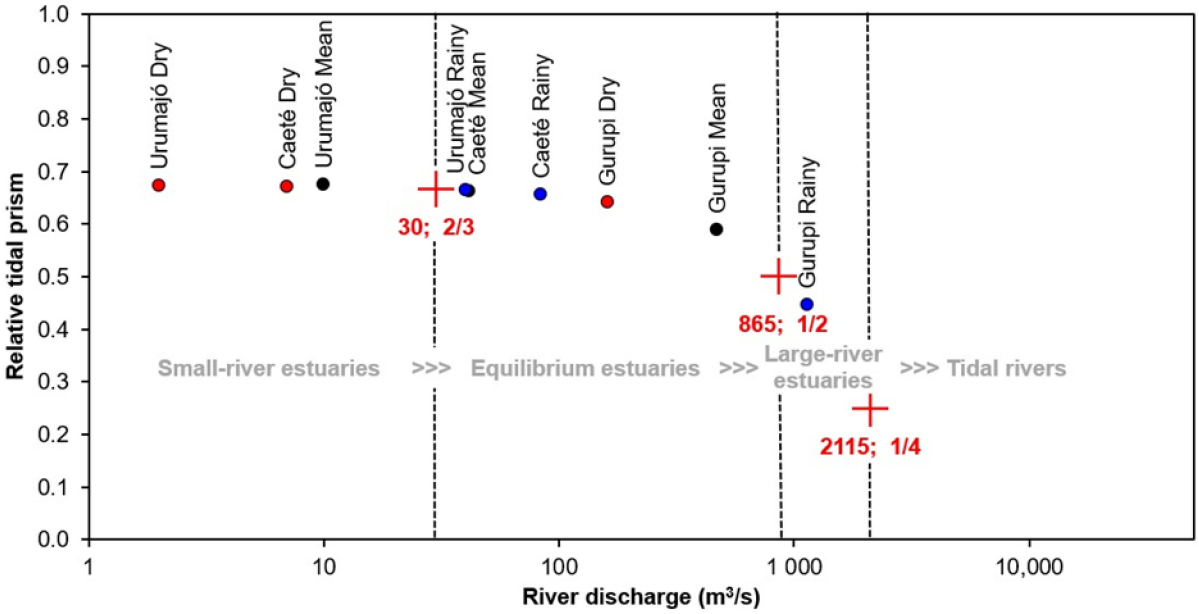

Figure 10. Correlation of relative tidal prism and fluvial discharge of the Gurupi estuary based on the seasonal variations of fluvial discharge, in comparison to the Caeté and Urumajó estuaries (data from [18]). The red circles represent the dry season, the blue circles represent the rainy season and the black circles represent the mean river discharge values. River discharge is represented in a logarithmic scale.

The dominant provenance (fluvial or marine) of sediments accumulated in macrotidal estuaries can also be used to classify an estuary. When the accumulating sediment is primarily sourced from the river the estuary is classified as a bypassing type, usually corresponding to a river-dominated estuary. When the accumulating sediment is primarily sourced offshore the estuary is classified a starve type, typically corresponding to a tide-dominated estuary [59]. The Gurupi River provides a small amount of sediment, and therefore, it could not be referred to as a river-dominated estuary. Instead, we refer to the Gurupi as a large river estuary. It was also considered that with a similar physical setting, a fluvial discharge of ~2115 $m^3 \cdot s^{-1}$ would imply a relative tidal prism as small as one-quarter of the total estuarine volume (Figure 10). In this case, it was assumed that such a system would be classified as a tidal river.

The tidal propagation can also be used to compare and classify estuaries. When the tidal wave propagates landward without significant changes in amplitude, the estuary is classified as synchronous, for example, the Mocajuba estuary [18]. When the tidal wave attenuates landward, the estuary is classified as hyposynchronous, and an example is the Taperaçu estuary [18]. In the Gurupi estuary an effect of tidal amplification is observed, indicating hypersynchronous behavior (Figure 5). The same effect was also observed in the Caeté [6,18] and Urumajó estuaries [18,24]. This landward tidal amplification likely contributes to the import of sediment in all of these ARP-influenced systems.

Another important aspect of tidal properties is phase asymmetry. Ebb–flood duration or magnitude asymmetries are caused by the tidal wave distortion [60,61]. Shorter phases would normally result in higher velocities and therefore, a higher sediment transport in that phase. This is the case for the Gurupi estuary during the dry season, which exhibits an ebb dominance. However, during the rainy season, current velocities were higher during the (longer) ebb phase, reinforcing the large impact of the fluvial discharge. This pattern has not been documented for other estuaries of the region, with smaller fluvial discharges. The morphology has a large impact on the flood/ebb tidal asymmetry. Bottom friction promotes the tidal flood duration asymmetry, while the accumulation of sediments

promotes the tidal ebb duration asymmetry [61–64]. The Gurupi morphology, which does not substantially change seasonally, promotes shorter flood phases in both seasons.

6. Conclusions

This work demonstrates the complexity of estuarine morphology and hydrodynamics, especially in a region dominated by the Amazon River Plume. The Gurupi is a shallow, coastal plain estuary, with a typical tide-controlled morphology, which results in substantial deformation of the tidal wave as it propagates upstream. Despite a macrotidal regime, the Gurupi is classified as a partially mixed estuary due to estuarine stratification analysis [15].

Seasonal variation had a great influence on the dynamics of the Gurupi estuary. Although an ETM occurred during both seasons, its location and concentration changed significantly. During the dry season, the ETM moved landward, and the SSC was substantially higher in comparison to the rainy season. The salinity and SSCs were substantially higher throughout the estuary during the dry season, and as a result, reduced fluvial discharge resulted in the concentration/accumulation of suspended sediments.

The large fluvial discharge associated with the estuarine morphology affected the current velocities and the tidal phase duration. In both seasons, the Gurupi morphology promoted shorter flood phases. However, the fluvial discharge during the rainy season resulted in higher current velocities during the (longer) ebb phase. The estuarine exchange was the dominant driver of the net sediment flux in both seasons. The estuary imported suspended sediments, though the net sediment fluxes were difficult to establish during the rainy season.

Overall, the results showed that the combination of sediment supply, hydrodynamics, and morphology placed the Gurupi in a peculiar situation between river and tidal domination. Although the high fluvial discharge affects the estuarine dynamics, it does not result in substantial fluvial sediment input, whereas we suggest the term large river, tide-dominated estuary. The partial stratification and seasonal ebb dominance of the flow are directly related to the increased fluvial discharge and highlight the importance of freshwater input along the Amazon coast and its large mangrove areas.

Author Contributions: Conceptualization, A.M.M.S., A.S.O. and N.E.A.; methodology, A.M.M.S., H.E.G., M.E.J., V.J.C.G., A.S.O. and N.E.A.; validation, A.S.O. and N.E.A.; formal analysis, A.M.M.S., H.E.G., V.J.C.G., A.S.O. and N.E.A.; investigation, A.M.M.S., H.E.G., M.E.J., V.J.C.G., A.S.O. and N.E.A.; resources, A.S.O. and N.E.A.; data curation, A.M.M.S., V.J.C.G. and N.E.A.; writing original draft preparation, A.M.M.S., H.E.G., M.E.J., V.J.C.G., A.S.O. and N.E.A.; writing—review and editing, A.M.M.S., A.S.O. and N.E.A.; visualization, A.M.M.S., A.S.O. and N.E.A.; supervision, A.S.O. and N.E.A.; project administration, N.E.A.; funding acquisition, N.E.A. and A.S.O. All authors have read and agreed to the published version of the manuscript.

Funding: This research was funded by the Coordenação de Aperfeiçoamento de Pessoal de Nível Superior (CAPES), via the IODP/CAPES-Brasil (0553/2015) and Pro-Amazônia (3290/2013) programs, as well as by the Conselho Nacional de Desenvolvimento Científico e Tecnológico—CNPq (446895/2014-8 and 307182/2018-5). Nils E. Asp is a CNPq research fellow. A.S.O, H.E.G. and M.E.J. were supported via the Office of Naval Research Grant N000141712350. PROPESP/UFPA (PAPQ) was responsible for the payment of the Article Processing Charge (APC).

Data Availability Statement: The data presented in this study are available on request from the corresponding author. The data are not publicly available due to the current lack of an adequate public databank and partially being considered for publication in an upcoming thesis.

Acknowledgments: We are thankful to the Brazilian and U.S.A. research institutions, especially the National Council for Scientific and Technological Development (CNPq) and the Coordination of Improvement of Higher Education Personnel (CAPES) for the financial support of the project and the student research grants. Additionally, we thank the LAGECO and School of Oceanography staff for their contributions to the fieldwork and laboratory analyses. We also thank the PAPQ program from PROPESP/UFPA for the APC funding.

Conflicts of Interest: The authors declare no conflict of interest.

References

1. Syvitski, J.P.M.; Kettner, A. Sediment Flux and the Anthropocene. *Philos. Trans. R. Soc. A Math. Phys. Eng. Sci.* **2011**, *369*, 957–975. [CrossRef]
2. Nowacki, D.J.; Ogston, A.S.; Nittrouer, C.A.; Fricke, A.T.; Van, P.D.T. Sediment Dynamics in the Lower Mekong River: Transition from Tidal River to Estuary. *J. Geophys. Res. Ocean* **2015**, *120*, 6363–6383. [CrossRef]
3. Milliman, J.D.; Farnsworth, K.L. *River Discharge to the Coastal Ocean: A Global Synthesis*; Cambridge University Press: Cambridge, UK, 2011.
4. Meade, R.H.; Nordin, C.F.; Curtis, W.F.; Costa Rodrigues, F.M.; do Vale, C.M.; Edmond, J.M. Sediment Loads in the Amazon River. *Nature* **1979**, *278*, 161–163. [CrossRef]
5. Souza Filho, P.W.M. Costa de Manguezais de Macromaré Da Amazônia: Cenários Morfológicos, Mapeamento e Quantificação de Áreas Usando Dados de Sensores Remotos. *Rev. Bras. Geofís.* **2005**, *23*, 427–435. [CrossRef]
6. Asp, N.E.; Gomes, V.J.C.; Schettini, C.A.F.; Souza-Filho, P.W.M.; Siegle, E.; Ogston, A.S.; Nittrouer, C.A.; Silva, J.N.S.; Nascimento, W.R.; Souza, S.R.; et al. Sediment Dynamics of a Tropical Tide-Dominated Estuary: Turbidity Maximum, Mangroves and the Role of the Amazon River Sediment Load. *Estuar. Coast. Shelf Sci.* **2018**, *214*, 10–24. [CrossRef]
7. Souza Filho, P.W.M.; Lessa, G.C.; Cohen, M.C.L.; Costa, F.R.; Lara, R.J. The Subsiding Macrotidal Barrier Estuarine System of the Eastern Amazon Coast, Northern Brazil. In *Geology and Geomorphology of Holocene Coastal Barriers of Brazil*; Lecture Notes in Earth Sciences; Springer: Berlin/Heidelberg, Germany, 2009; Volume 107, pp. 347–375. ISBN 9783540250081.
8. Cohen, M.C.L.; Souza Filho, P.W.M.; Lara, R.J.; Behling, H.; Angulo, R.J. A Model of Holocene Mangrove Development and Relative Sea-Level Changes on the Bragança Peninsula (Northern Brazil). *Wetl. Ecol. Manag.* **2005**, *13*, 433–443. [CrossRef]
9. Sioli, H. The Amazon and Its Main Affluents: Hydrography, Morphology of the River Courses, and River Types. In *The Amazon: Limnology and Landscape Ecology of a Mighty Tropical River and Its Basin*; Sioli, H., Ed.; Springer: Dordrecht, The Netherlands, 1984; pp. 127–165.
10. Copeland, B. Effects of Decreased River Flow on Estuary Ecology. *Water Pollut. Control Fed.* **1966**, *38*, 1831–1839.
11. Ridderinkhof, H. Sediment Transport in Intertidal Areas. In *Intertidal Deposits: River Mouths, Tidal Flats, and Coastal Lagoons*; Eisma, D., Ed.; CRC Press: Boca Raton, FL, USA, 1998; pp. 363–382. ISBN 0-8493-8049-9.
12. Zhang, E.; Savenije, H.H.G.; Wu, H.; Kong, Y.; Zhu, J. Analytical Solution for Salt Intrusion in the Yangtze Estuary, China. *Estuar. Coast. Shelf Sci.* **2011**, *91*, 492–501. [CrossRef]
13. Zhang, E.F.; Savenije, H.H.G.; Chen, S.L.; Mao, X.H. An Analytical Solution for Tidal Propagation in the Yangtze Estuary, China. *Hydrol. Earth Syst. Sci.* **2012**, *16*, 3327–3339. [CrossRef]
14. Cai, H.; Savenije, H.H.G.; Toffolon, M. Linking the River to the Estuary: Influence of River Discharge on Tidal Damping. *Hydrol. Earth Syst. Sci.* **2014**, *18*, 287–304. [CrossRef]
15. Geyer, W.R.; MacCready, P. The Estuarine Circulation. *Annu. Rev. Fluid. Mech.* **2014**, *46*, 175–197. [CrossRef]
16. Martins, E.D.S.F.; Souza Filho, P.W.M.; Costa, F.R.; Alves, P.J.O. Extração Automatizada e Caracterização Da Rede de Drenagem e Das Bacias Hidrográficas Do Nordeste Do Pará Ao Noroeste Do Maranhão a Partir de Imagens SRTM. In Proceedings of the 13 Simpósio Brasileiro de Sensoriamento Remoto, Florianópolis, Brazil, 21–26 April 2007; pp. 6827–6834.
17. Asp, N.E.; Gomes, J.D.; Gomes, V.J.C.; Omachi, C.Y.; Silva, A.M.M.; Siegle, E.; Serrao, P.F.; Thompson, C.C.; Nogueira, L.C.; Francini-Filho, R.B.; et al. Water Column and Bottom Gradients on the Continental Shelf Eastward of the Amazon River Mouth and Implications for Mesophotic Reef Occurrence. *J. Mar. Syst.* **2022**, *225*, 103642. [CrossRef]
18. Gomes, V.J.C.; Asp, N.E.; Siegle, E.; Gomes, J.D.; Silva, A.M.M.; Ogston, A.S.; Nittrouer, C.A. Suspended-Sediment Distribution Patterns in Tide-Dominated Estuaries on the Eastern Amazon Coast: Geomorphic Controls of Turbidity-Maxima Formation. *Water* **2021**, *13*, 1568. [CrossRef]
19. Araújo, T.C.M.; Seoane, J.C.S.; Coutinho, P.N. Geomorfologia Da Plataforma Continental de Pernambuco. In *Oceanografia: Um Cenário Tropical*; Leça, E.E., Neumann-Leitão, S., Costa, M.F., Eds.; Bagaço: Recife, Brazil, 2004; pp. 39–57.
20. Coles, V.J.; Brooks, M.T.; Hopkins, J.; Stukel, M.R.; Yager, P.L.; Hood, R.R. The Pathways and Properties of the Amazon River Plume in the Tropical North Atlantic Ocean. *J. Geophys. Res. Ocean* **2013**, *118*, 6894–6913. [CrossRef]
21. Goes, J.I.; do Rosario Gomes, H.; Chekalyuk, A.M.; Carpenter, E.J.; Montoya, J.P.; Coles, V.J.; Yager, P.L.; Berelson, W.M.; Capone, D.G.; Foster, R.A.; et al. Influence of the Amazon River Discharge on the Biogeography of Phytoplankton Communities in the Western Tropical North Atlantic. *Prog. Oceanogr.* **2014**, *120*, 29–40. [CrossRef]
22. Geyer, W.R.; Beardsley, R.C.; Lentz, S.J.; Candela, J.; Limeburner, R.; Johns, W.E.; Castro, B.M.; Soares, I.D. Physical Oceanography of the Amazon Shelf. *Cont. Shelf Res.* **1996**, *16*, 575–616. [CrossRef]
23. Nittrouer, C.A.; Kuehl, S.A.; Sternberg, R.W.; Figueiredo, A.G.; Faria, L.E.C. An Introduction to the Geological Significance of Sediment Transport and Accumulation on the Amazon Continental Shelf. *Mar. Geol.* **1995**, *125*, 177–192. [CrossRef]
24. Asp, N.E.; Gomes, V.J.C.; Ogston, A.; Borges, J.C.C.; Nittrouer, C.A. Sediment Source, Turbidity Maximum, and Implications for Mud Exchange between Channel and Mangroves in an Amazonian Estuary. *Ocean Dyn.* **2016**, *66*, 285–297. [CrossRef]
25. Asp, N.E.; Amorim de Freitas, P.T.; Gomes, V.J.C.; Gomes, J.D. Hydrodynamic Overview and Seasonal Variation of Estuaries at the Eastern Sector of the Amazonian Coast. *J. Coast. Res.* **2013**, *165*, 1092–1097. [CrossRef]
26. Cohen, M.C.L.; Lara, R.J.; Ramos, J.D.F.; Dittmar, T. Factors Influencing the Variability of Mg, Ca and K in Waters of a Mangrove Creek in Braganca, North Brazil. *Mangroves Salt Marshes* **1999**, *3*, 9–15. [CrossRef]

27. Pereira, C.T.C.; Giarrizzo, T.; Jesus, A.J.S.; Martinelli, J.M. Caracterização Do Efluente de Cultivo de Litopenaeus Vannamei No Estuário Do Rio Curuçá (PA). In *Sistemas de Cultivos Aqüícolas na Zona Costeira do Brasil: Recursos, Tecnologias, Aspectos Ambientais e Sócio-Econômicos*; Barroso, G.F., Poersch, L.H.S., Cavalli, R.O., Eds.; Editora do Museu Nacional: Rio de Janeiro, Brazil, 2007; pp. 291–301.
28. Lima, I.F.; Prata, T.C.; Maria, A.; Lima, M. de Análise Da Paisagem Aplicada a Bacia Do Rio Gurupi Pa/Ma. In Proceedings of the XXII Simpósio Brasileiro de Recursos Hídricos, Florianópolis, Brazil, 16 November–1 December 2017; pp. 1–8.
29. Gomes, J.D. *Caracterização Hidrodinâmica Do Estuário Do Rio Gurupi, Na Zona Costeira Amazônica*; Universidade Federal do Pará: Belém, Brazil, 2015.
30. Figueroa, S.N.; Nobre, C.A. Precipitations Distribution over Central and Western Tropical South América. *Climanál.-Bol. Monit. Anál. Clim.* **1990**, *5*, 36–45.
31. Marengo, J.A. Interannual Variability of Deep Convection over the Tropical South American Sector as Deduced from ISCCP C2 Data. *Int. J. Climatol.* **1995**, *15*, 995–1010. [CrossRef]
32. de Moraes, B.C.; da Costa, J.M.N.; da Costa, A.C.L.; Costa, M.H. Variação Espacial e Temporal Da Precipitação No Estado Do Pará. *Acta Amaz.* **2005**, *35*, 207–214. [CrossRef]
33. Gomes, V.J.C.; Freitas, P.T.A.; Asp, N.E. Dynamics and Seasonality of the Middle Sector of a Macrotidal Estuary. *J. Coast Res.* **2013**, *165*, 1140–1145. [CrossRef]
34. ANA—Agência Nacional de Águas. Hidroweb: Serviço de Informações Hidrológicas. Available online: http://www3.ana.gov.br (accessed on 11 December 2020).
35. Strickland, J.D.H.; Parsons, T.R. *A Practical Handbook of Seawater Analysis*, 2nd ed.; Fisheries Research Board of Canada Bulletin: Ottawa, ON, Canada, 1972; Volume 167.
36. Glover, H.E.; Ogston, A.S.; Fricke, A.T.; Nittrouer, C.A.; Aung, C.; Naing, T.; Kyu Kyu, K.; Htike, H. Connecting Sediment Retention to Distributary-Channel Hydrodynamics and Sediment Dynamics in a Tide-Dominated Delta: The Ayeyarwady Delta, Myanmar. *J. Geophys. Res. Earth Surf.* **2021**, *126*, e2020JF005882. [CrossRef]
37. Giddings, S.N.; Monismith, S.G.; Fong, D.A.; Stacey, M.T. Using Depth-Normalized Coordinates to Examine Mass Transport Residual Circulation in Estuaries with Large Tidal Amplitude Relative to the Mean Depth. *J. Phys. Ocean* **2014**, *44*, 128–148. [CrossRef]
38. McLachlan, R.L.; Ogston, A.S.; Allison, M.A. Implications of Tidally-Varying Bed Stress and Intermittent Estuarine Stratification on Fine-Sediment Dynamics through the Mekong's Tidal River to Estuarine Reach. *Cont. Shelf Res.* **2017**, *147*, 27–37. [CrossRef]
39. Lerczak, J.A.; Geyer, W.R.; Chant, R.J. Mechanisms Driving the Time-Dependent Salt Flux in a Partially Stratified Estuary. *J. Phys. Ocean* **2006**, *36*, 2296–2311. [CrossRef]
40. Sternberg, R.W. Friction Factors in Tidal Channels with Differing Bed Roughness. *Mar. Geol.* **1968**, *6*, 243–260. [CrossRef]
41. Ginestet, C. Ggplot2: Elegant Graphics for Data Analysis. *J. Stat. Softw.* **2009**, *35*, 245. [CrossRef]
42. Oksanen, J. Vegan: An Introduction to Ordination. *Management* **2008**, *1*, 1–10.
43. R Core Team. *A Language and Environment for Statistical Computing*; R Foundation for Statistical Computing: Vienna, Austria, 2020.
44. Royston, P. Approximating the Shapiro-Wilk W-Test for Non-Normality. *Stat. Comput.* **1992**, *2*, 117–119. [CrossRef]
45. Sheskin, D.J. The Mann–Whitney U Test. In *Handb. Parametr. Nonparametric Stat. Proced*, 5th ed.; Sheskin, D.J., Ed.; Chapman and Hall/CRC: New York, NY, USA, 2011; pp. 531–594. [CrossRef]
46. Wilcoxon, F. Individual Comparisons by Ranking Methods. In *Breakthroughs in Statistics*; Springer: New York, NY, USA, 1992; pp. 196–202.
47. Wu, J.; Liu, J.T.; Wang, X. Sediment Trapping of Turbidity Maxima in the Changjiang Estuary. *Mar. Geol.* **2012**, *303–306*, 14–25. [CrossRef]
48. Dyer, K.R. *Estuaries: A Physical Introduction*, 2nd ed.; Wiley-Interscience Publication; John Wiley and Sons: New York, NY, USA, 1997; ISBN 0-471-9741-4.
49. Allen, G.P.; Salomon, J.C.; Bassoullet, P.; du Penhoat, Y.; de Grandpre, C. Effects of Tides on Mixing and Suspended Sediment Transport in Macrotidal Estuaries. *Sediment. Geol.* **1980**, *26*, 69–90. [CrossRef]
50. Jay, D.A.; Dungan Smith, J.; Jay, D.; SMrrH, J. Circulation, Density Distribution and Neap-Spring Transitions in the Columbia River Estuary. *Prog. Oceanogr.* **1990**, *25*, 81–112. [CrossRef]
51. Uncles, R.J.; Stephens, J.A.; Law, D.J. Turbidity Maximum in the Macrotidal, Highly Turbid Humber Estuary, UK: Flocs, Fluid Mud, Stationary Suspensions and Tidal Bores. *Estuar. Coast. Shelf Sci.* **2006**, *67*, 30–52. [CrossRef]
52. Valerio, A.M.; Kampel, M.; Ward, N.D.; Sawakuchi, H.O.; Cunha, A.C.; Richey, J.E. CO2 Partial Pressure and Fluxes in the Amazon River Plume Using in Situ and Remote Sensing Data. *Cont. Shelf Res.* **2021**, *215*, 104348. [CrossRef]
53. Silva, A.M.M.; Asp, N.E.; Gomes, V.J.C.; Ogston, A.S. Impacts of Inherited Morphology and Offshore Suspended-Sediment Load in an Amazon Estuary. *Estuar. Coasts* **2023**. (*under review*).
54. Geyer, W.R. Estuarine Salinity Structure and Circulation. In *Contemporary Issues in Estuarine Physics*; Valle-Levinson, A., Ed.; Cambridge University Press: Cambridge, UK, 2010; pp. 22–26.
55. Hansen, D.V.; Rattray, M. New Dimensions in Estuary Classification. *Limnol. Oceanogr.* **1966**, *11*, 319–326. [CrossRef]
56. Valle-Levinson, A. Definition and Classification of Estuaries. In *Contemporary Issues in Estuarine Physics*; Valle-Levinson, A., Ed.; Cambridge University Press: Cambridge, UK, 2010; pp. 1–11.
57. Farmer, D.M.; Freeland, H.J. The Physical Oceanography of Fjords. *Prog. Oceanogr.* **1983**, *12*, 147–220. [CrossRef]

58. Lessa, G.C.; Santos, F.M.; Souza Filho, P.W.; Corrêa-Gomes, L.C. Brazilian Estuaries: A Geomorphologic and Oceanographic Perspective. In *Brazilian Estuaries: A Benthic Perspective*; Lana, P.D.C., Bernardino, A.F., Eds.; Springer International Publishing: Cham, Switzerland, 2018; pp. 1–37. ISBN 978-3-319-77779-5.
59. Chappell, J.; Woodroffe, C.D. Macrotidal Estuaries. In *Coastal Evolution: Late Quaternary Shoreline Morphodynamics*; Carter, R.W.G., Woodroffe, C.D., Eds.; Cambridge University Press: Cambridge, UK, 1994; pp. 187–218.
60. Dronkers, J. Tidal Asymmetry and Estuarine Morphology. *Neth. J. Sea Res.* **1986**, *20*, 117–131. [CrossRef]
61. Kang, J.W.; Jun, K.S. Flood and Ebb Dominance in Estuaries in Korea. *Estuar. Coast. Shelf Sci.* **2003**, *56*, 187–196. [CrossRef]
62. Aubrey, D.G.; Speer, P.E. A Study of Non-Linear Tidal Propagation in Shallow Inlet/Estuarine Systems Part I: Observations. *Estuar. Coast Shelf. Sci.* **1985**, *21*, 185–205. [CrossRef]
63. Brown, J.M.; Davies, A.G. Flood/Ebb Tidal Asymmetry in a Shallow Sandy Estuary and the Impact on Net Sand Transport. *Geomorphology* **2010**, *114*, 431–439. [CrossRef]
64. Friedrichs, C.T.; Aubrey, D.G. Nonlinear Tidal Distortion in Shallow Well-Mixed Estuaries. *Estuar. Coast Shelf. Sci.* **1988**, *27*, 521–545. [CrossRef]